Passing the Alfvén Layer by Means of Chorus Acceleration

Hayley J. Allison[1], Yuri Y. Shprits[1,2,3], Dedong Wang[1], Michael Wutzig[1], Richard B. Horne[4], Sarah A. Glauert[4], Alexander Drozdov[3]

[1]GFZ Helmholtz Centre, Potsdam, Germany
[2]Institute of Physics and Astronomy, University of Potsdam, Potsdam, Germany
[3]Department of Earth, Planetary and Space Sciences, University of California, Los Angeles, CA, USA
[4]British Antarctic Survey, Cambridge, UK

Key Points:

- 2-D and 4-D simulations are performed to explore chorus acceleration time scales in comparison to electron drift times
- Chorus waves can accelerate electrons on open drift paths so that they remain trapped in the system
- The energy distribution of the electrons contributes to whether they can be accelerated within the drift time by chorus interactions

Corresponding author: Hayley J. Allison, `haylis@gfz-potsdam.de`

Abstract

Sustained periods of southward interplanetary magnetic field can result in strong magnetospheric convection, during which, the Alfvén layer, separating regions of sunward convection and closed drift paths, migrates earthwards. Plasmasheet electrons then have direct access to the inner magnetosphere, traversing the dawn sector before crossing the magnetopause, and present a potential seed population for the radiation belts. Here we examine, for the first time, whether energetic electrons can be sufficiently energised during their drift, via resonant interactions with whistler-mode chorus waves, so as to pass the Alfvén layer prior to leaving the system. We utilise a natural coordinate system for magnetosphere convection, (U,B,K) space, in which we calculate the drift trajectories, electron energies on open drift paths, and drift times. The acceleration time from resonant chorus-wave particle interactions is calculated using the Versatile Electron Radiation Belt model (VERB) first as a 2-D diffusion equation and then in 4-D convection-diffusion mode. Comparing the drift times to the acceleration timescales we find that interactions with chorus waves do result in a portion of the electrons on open drift paths passing the Alfvén energy. However, whether this acceleration occurs sufficiently quickly depends on the energy distribution of the electron population.

1 Introduction

Owing to the entropy simlarities and correlations between plasmasheet and radiation belt populations (Burin des Roziers et al., 2009; Borovsky & Cayton, 2011), Earth's electron radiation belts are generally considered to be formed from plasmasheet electrons, supplied to the inner magnetosphere and energised by processes such as inward radial diffusion and local acceleration (Horne et al., 2005; Shprits, Elkington, et al., 2008). The circumstances under which these electrons are supplied are still not fully understood, and enhancements are seen associated with substorm injections (DeForest & McIlwain, 1971) as well as in the absence of substorm activity (Kissinger et al., 2014). Periods of enhanced convection and substorm injections are typically thought to introduce enhancements in the $\sim$1 - 100s keV electron energy range. These source (1-10s keV) and seed (10s - 100s keV) electrons are a vital part of radiation belt dynamics, with enhancements suppressed when either of these components is absent (Jaynes et al., 2015).

For electrons at source and seed energies, the drift motion is impacted by the electric field configuration to a much greater degree than electrons at relativistic energies. Due to the enhanced convection electric field during active periods, these source and seed electrons can drift out to the magnetopause (so-called 'open' drifts), resulting in magnetic local time dependent distributions in the electron flux (Allison et al., 2017; Thorne et al., 2007), whereas, for the same starting location, relativistic electrons would encircle the Earth (closed drifts). The relaxation of the electric and magnetic field configuration on time frames less than the particle's drift period retains electrons on open drift paths, allowing source and seed population to be energised over multiple drift periods (Lyons & Williams, 1984). Alternatively, there is a finite window of time for electrons on open drift paths to be accelerated up to trapped energies (past the Alfvén layer) and contribute to radiation belt enhancements; a time frame approximately equal to half the drift period.

One energisation mechanism in Earth's radiation belt region is resonant wave-particle interactions with electromagnetic whistler mode chorus waves. Chorus diffusion coefficients indicate that electrons with energies of 10s-100s keV are strongly influenced by chorus wave activity (e.g. Horne et al., 2013), undergoing both acceleration and pitch angle scattering. Horne et al. (2005) showed that at electron energies less than $\sim$300 keV, interactions with chorus waves result in a competition between acceleration and loss, whereas, above $\sim$300 keV, acceleration occurs faster than loss. However, the balance between acceleration and loss depends on a number of factors (Wang & Shprits, 2019), including the energy distribution of the electron population. For certain conditions <300 keV electrons can exhibit acceleration by chorus waves (Allison et al., 2019). How this acceleration time scale compares to the particle drift times, which for 1-100s keV electrons can be several hours, has thus far not been tested.

In this work, we address whether it is possible to retain a portion of the seed population, on open drift paths, via chorus acceleration. The primary assumption here is that the fields remain static, throughout the particle drift time. In reality this is not necessarily the case, however, by making this assumption we isolate the contribution of chorus wave acceleration alone. In Section 2, we calculate the Alfvén layer energies at various locations about the Earth, under different magnetic and electric field conditions to determine the energy threshold of trapped electrons. In Section 3, we compute drift times for these particles to move from the nightside to the noon sector. Sections 4 and 5 then respectively use 2-D or 4-D modelling to examine whether electrons pass the threshold energies, via chorus acceleration, within the drift time.

2 Energies of the Alfvén layer

The smallest electron energy on a closed drift path can be calculated using the coordinate system introduced by Whipple Jr. (1978): electric potential U, magnetic field intensity B, and invariant K space. Several authors have previously made use of this convention (e.g. Mouikis et al., 2019; Bingham et al., 2019; Korth et al., 1999; Korth & Thomsen, 2001), which describes the drift trajectories arising from $E\times B$ drift and gradient and curvature drift by a Hamiltonian energy conservation. A particle conserving the first two invariants also conserves its total energy, and Whipple Jr. (1978) showed that

$$\frac{\partial U}{\partial B_m} = -\frac{\mu}{q} \tag{1}$$

where $B_m(K)$ is the field strength at the mirror point for a particle with invariant K, q retains the sign of the particle charge, and μ denotes the first adiabatic invariant, which can be calculated with

$$\mu = \frac{p_\perp^2}{2mB}. \tag{2}$$

As the solution to Equation 1 is $U = (-\mu/q)B_m + \textit{constant}$, all particle drift trajectories in the (U, B, K) space are straight lines with gradient $-\mu/q$.

For a dipole magnetic field, the equatorial field strength is given by $B_{eq}(r) = B_0 R_E^3/r^3$, where B_0 is the magnetic field at the equator at the Earth's surface (taken to be $0.3\times10^{-4}\ T$). These dipole equations can be substituted into the (Volland, 1973);(Stern, 1975) electric field to produce the potential

$$U = -E_0 R_E^\gamma \left(\frac{B_0}{B_{eq}}\right)^{\gamma/3} \sin(\phi) - \frac{a}{R_E}\left(\frac{B_{eq}}{B_0}\right)^{1/3} \tag{3}$$

which has a maximum along the dawn terminator (where $\phi = -\pi/2$) and a minimum on the dusk terminator (where $\phi = \pi/2$). Using the (Maynard & Chen, 1975) parameterization, a is a Kp dependent factor related to the convection electric field strength and γ is a parameter set equal to 2.

In a Volland (1973); Stern (1975) electric field and dipole magnetic field, the mapping into the (U, B, K) space is double valued, representing opposite sides of the dawn-dusk meridian. We use this electric and magnetic field configuration for the calculations in this paper. The simplest scenario for Equation 1 occurs when $K = 0\ G^{1/2}R_E$, in which all particles are equatorially mirroring, $B_m = B_{eq}$, and only the equatorial plane need be considered. In the following calculations, we assume $K = 0\ G^{1/2}R_E$ for simplicity. At our chosen value of K, the straight line trajectories that intersect both the dawn and dusk potential extremes will be on closed paths, while trajectories which intersect only

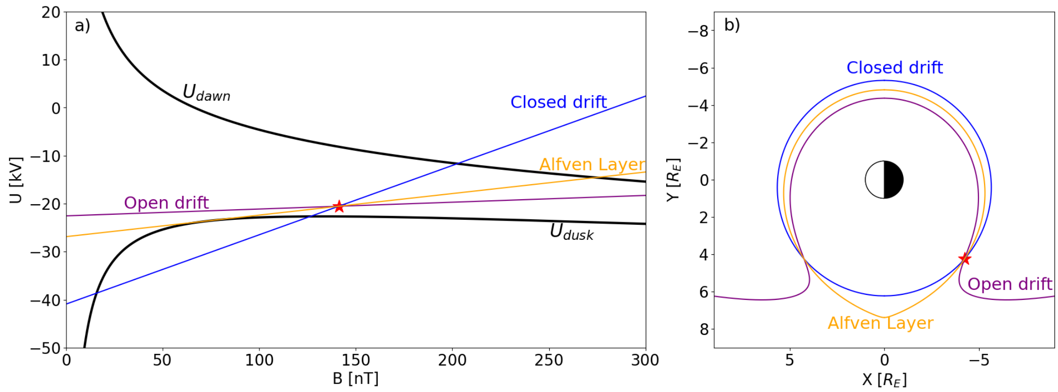

Figure 1. An illustration of three drifts in the (U, B, $K = 0$) coordinate system for electrons (panel a). All three electron drifts shown are for Kp = 3 in a Volland (1973);Stern (1975) electric field with a Maynard and Chen (1975) Kp parameterization, starting at MLT = 21 and L = 5.5, marked by the red star. The orange line shows the electron Alfvén layer, the blue line a closed drift path, and the purple an open drift path. The lines labelled U_{dusk} and U_{dawn} on Panel a show the potential at the dusk and dawn points respectively. Panel b illustrates the spatial drifts corresponding to these three lines.

one extreme will have an open drift path. Figure 1 shows the (U, B, K) lines and corresponding drift paths for electrons with $K = 0\ G^{1/2}R_E$. For a particular location, the electron Alfvén layer is the trajectory in (U, B, K) space which first glances the dusk potential (see the orange line labelled 'Alfvén layer'). As the gradient of the trajectory is $-\mu/q$, we therefore seek the smallest value of μ, and therefore energy, for which this is the case.

At each point on the equatorial plane, the gradient of the line corresponding to the Alfvén layer, and hence the smallest energy on a closed drift path, is found by iteration. For the selected starting location, the corresponding U-B_{eq} coordinates are calculated, and an initial energy of 1 keV is selected to compute the starting value of μ. We then iteratively increase the gradient until the trajectory's approach to the dusk potential is within a selected dE threshold. In this work, we select $dE = 0.1$ keV, and the Alfvén layer energies are therefore accurate to 0.1 keV. Electrons on drifts which pass the dusk sector, travelling anti-clockwise, will never see the dawn potential. This situation manifests in U-B_{eq} space as a starting B value which is lower than the B value at which U_{dusk} is crossed (see Supplementary Figure S1). By implementing this check, we can determine when dusk-line orbits occur.

Using the Volland (1973);Stern (1975) electric field with the Maynard and Chen (1975) Kp parametrisation and a dipole magnetic field, we show the minimum trapped energy of equatorially mirroring electrons as a function of MLT and L for 9 values of Kp in Figure 2. If the minimum energy lies below 1 keV, it was not plotted. There are two ways to interpret the energy cut-off values shown. They are both the lowest trapped energy, and they are also the highest energy electron which can access that location from the plasmasheet, purely from convective motion. Previous work has primarily taken the later interpretation (Korth et al., 1999; Korth & Thomsen, 2001), while we consider the former here.

Figure 2 shows that for low Kp values (Kp≤3), the lowest energy on a closed drift path is less than 60 keV for all MLT and L considered. As Kp increases, the threshold energy also increases, reaching 125 keV on the dawn side at L = 6 for Kp = 6. On the

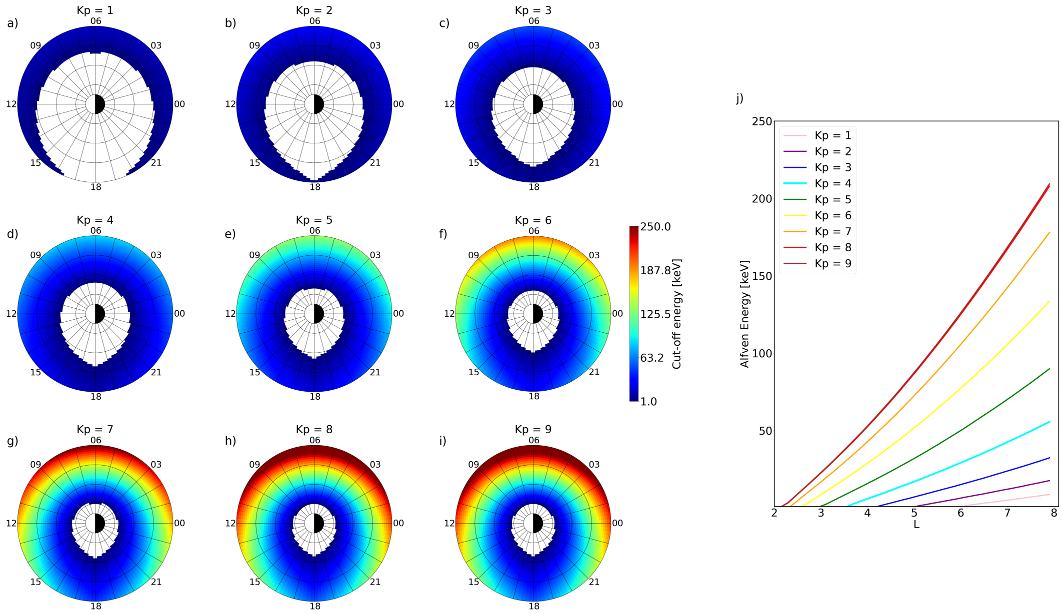

Figure 2. Lowest electron energies on closed drift paths at different locations about the Earth for nine levels of Kp (a-i), calculated for equatorially mirroring particles in a dipole magnetic field and Volland (1973);Stern (1975) electric field with a Maynard and Chen (1975) Kp parameterization. The outermost distance is $L = 8$, and tick marks for every $L = 2$ increment are shown. Where the lowest energy on a closed drift is below 1 keV, the energy is not plotted. Panel j shows the lowest energy on a closed drift path at MLT = 12 across L for 9 values of Kp (colored lines labelled in the legend).

dusk side, the threshold energy at L= 6, Kp=6 is markedly lower, 60 keV, suggesting that during enhanced convection, ∼60 keV electrons located on the dusk side at the commencement of the electric field enhancement can be retained over multiple drifts, while 60 keV electrons on the dawn side would be lost to the magnetopause. At the highest values of Kp studied, 7≤ Kp ≤ 9, the threshold energy on the dawn side is >125 keV for much of the outer belt region, between L = 4-6. At the highest dawn side radial distances, this can even extend to energies >250 keV.

As we are interested in whether electrons can be accelerated past the cut off energy within half a drift period, we focus on the Alfvén layer energies around noon. Electrons approaching noon will have drifted through the dawn sector and likely encountered chorus wave activity. Figure 2j shows these cut-off energies across L, at MLT = 12, for 9 levels of Kp. Open electron drift paths pass through MLTs other than MLT = 12 (Allison et al., 2017) and chorus waves are observed at MLTs past noon (Horne et al., 2013).Electrons can be lost at lower MLTs (which have higher Alfvén layer energies) as well at higher MLTs (with lower Alfvén layer energies). However, we use the threshold energies at an MLT of noon here as it provides a middle case. At MLT = 12, Figure 2j shows that between L = 4-5 the Alfvén layer energy is <100 keV for all values of Kp, and <10s keV for Kp < 5. For L > 5, we identify larger Alfvén layer energies, which can pass 100 keV, and show a greater dependence on Kp.

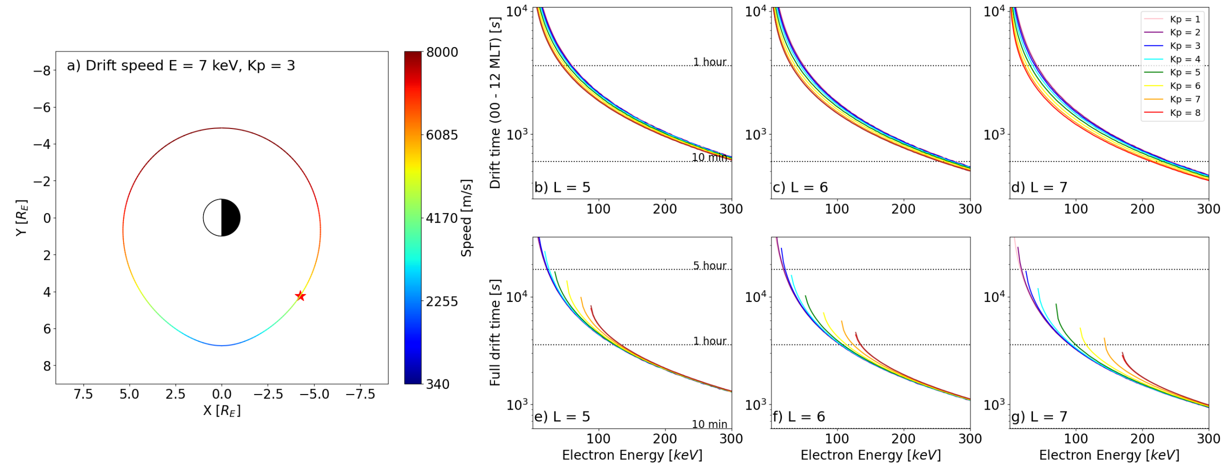

Figure 3. Using (U,B,K) coordinates and the drift speed, the drift time is calculated for 1-300 keV electrons under various electric field conditions. Panel a shows the variation in the drift speed of a 7 keV electron starting it's drift trajectory at the red star, for a dipole magnetic field and an electric field configuration appropriate for Kp = 3. Drift times for an electron moving from MLT = 00 to MLT = 12, for starting locations of L= 5, 6, and 7 are plotted in panel b, c, and d respectively. The total drift time for electrons above the Alfvén layer starting at these values of L are then shown in panels e-g. All energies are initialised at MLT = 00.

3 Electron drift times

To evaluate whether electrons can be accelerated sufficiently quickly so as to pass the threshold energies calculated in Section 2 before being lost from the magnetosphere, we require their drift time frame. Previous work has provided equations to calculate the drift times for electrons moving under the influence of magnetic drifts (e.g. Walt, 1994), however, for seed population energies, the drift time frame will also be highly influenced by changes in the convection electric field. Here we exploit (U,B,K) space further to calculate the drift times for varying electric field strength. As we only consider electrons restricted to the equatorial plane (K = 0 $G^{1/2}R_E$), for each point along the particle's drift path, determined by the trajectory in (U,B,K) space, we calculate the drift velocity as the combination of the electric drift and gradient magnetic drift

$$\mathbf{v} = \left(\frac{\mathbf{E}\times\mathbf{B}}{B^2}\right) + \frac{\mu}{qB^2}\mathbf{B}\times\nabla B, \tag{4}$$

taking the magnitude to obtain the drift speed. Figure 3a shows the calculated drift speed for an equatorially mirroring 7 keV electron starting at the red star. As a result of the convection electric field, the speed varies substantially along the orbit, ranging between $\sim$8000 ms^{-1} on the dawn side to $\sim$350 ms^{-1} on the dusk side. The drift time, T, can be obtained by

$$T = \int \frac{r}{v} d\phi \tag{5}$$

where v is the drift speed, r is the radial distance to a point on the orbit, and ϕ is the angle through the drift. As shown in Figure 1, (U,B,K) space can be used to obtain the relationship between ϕ and r defining the drift path.

We use Equation 5 to determine the time taken for electrons to drift from midnight to noon as well as the time taken for the electron energies above the Alfvén layer to complete a full drift. The results are shown in Figure 3 for various starting electron energies at MLT = 00, under different electric field strengths, given by 9 values of Kp. We see that, as the electric field strength increases, the time for the electron to drift from MLT = 00 to MLT = 12 reduces (Figure 3b-d). However, conversely, as Kp increases, the total drift time increases (Figure 3e-g). An enhanced convection electric field forces electrons on to more "tear-drop" shaped orbits, and the dusk side drift speed is reduced. The electrons then spend more time on the dusk side of the Earth, which more than compensates for the speed increase on the dawn side. As a result, during active periods, we expect the seed population electrons to take longer to drift around the Earth, and to spend less overall time in the dawn-side active chorus region (Wang et al., 2019). The non-uniformity in the sector drift times is an important consideration for drift-averaging diffusion coefficients for use in radiation belt models (e.g. Orlova & Shprits, 2014; Glauert et al., 2014; Su et al., 2010; Subbotin et al., 2011). Roederer (1967) demonstrated that in a non-dipole magnetic field, particles can spend 2-3 times more time on the night-side than they do on the day side. Here we have only considered a dipole magnetic field model for simplicity, and our results highlights that the inclusion of the electric field further complicates this picture for seed population energies.

The MLT = 00 - MLT = 12 drift times in Figure 3 provide timescales for the acceleration to the Alfvén layer energy if the electron is to remain in the system. We now use these timeframes in the context of radiation belt modelling.

4 Acceleration by chorus: VERB-2D

Initially, to determine the acceleration time scales from whistler mode chorus wave interactions, we employ quasi-linear theory (Kennel & Engelmann, 1966) and use the Versatile Electron Radiation Belt model in 2-D (VERB-2D: Shprits, Subbotin, et al., 2008) to solve the Fokker-Planck equation for the evolution of the phase space density, f, in coordinates of relativistic momentum, p, and pitch angle, α:

$$\begin{aligned}\frac{\partial f}{\partial t} \quad &= \quad \frac{1}{p^2}\frac{\partial}{\partial p}\bigg|_{\alpha} p^2\left(D_{pp}\frac{\partial}{\partial p}\bigg|_{\alpha} f + D_{p\alpha}\frac{\partial}{\partial \alpha}\bigg|_{p} f\right) \\ &+ \frac{1}{T(\alpha)\sin(2\alpha)}\frac{\partial}{\partial \alpha}\bigg|_{p} T(\alpha)\sin(2\alpha)\left(D_{\alpha\alpha}\frac{\partial}{\partial \alpha}\bigg|_{p} f + D_{p\alpha}\frac{\partial}{\partial p}\bigg|_{\alpha} f\right) \\ &- \frac{f}{\tau}\end{aligned} \tag{6}$$

$T(\alpha)$ is a function relating to the bounce motion and, in the dipole magnetic field, used here can be approximated as

$$T(\alpha) = 1.3802 - 0.3198(\sin\alpha + \sin^2\alpha). \tag{7}$$

The final term of Equation 6 accounts for atmospheric loss due to Coulomb collisions in the loss cone, where the parameter τ is the electron lifetime, taken to be a quarter of the bounce time inside the loss cone and infinite outside. A time step of 3 minutes is used for the simulations, along with a grid resolution of 211 $\times$ 89 in p and α, respectively.

Four boundary conditions are required for the model, one at the maximum and minimum values of both p and α. At the minimum equatorial pitch angle boundary we use $f = 0$, assuming total loss to the atmosphere, while, at the maximum equatorial pitch angle (89^o), the gradient of f in pitch angle is set to zero. Relativistic momentum, p, is related to the kinetic energy and we set the minimum and maximum p boundary to correspond to 1 keV and 30 MeV respectively. At the maximum p boundary, $f = 0$ allowing no $\geq$30 MeV population to be present in the simulations. For the minimum energy boundary, we consider constant f at 1 keV, representative of steady convection of 1 keV electrons filling the dawn sector as fast as they are scattered/accelerated.

We consider two initial phase space density conditions for the VERB-2D model runs. Firstly, a soft energy spectrum is used, taking a power law form with a flux of 10^7 $cm^{-2}s^{-1}sr^{-1}keV^{-1}$

at 1 keV and a flux of 10^3 $cm^{-2}s^{-1}sr^{-1}keV^{-1}$ at 200 keV. Secondly, we consider a harder spectrum, given by a exponential distribution of the electron flux, with a flux of 10^7 $cm^{-2}s^{-1}sr^{-1}keV^{-1}$ at 1 keV and a flux of 10^3 $cm^{-2}s^{-1}sr^{-1}keV^{-1}$ at 250 keV. For both initial conditions, the flux distribution in energy was converted to phase space density by dividing by the momentum squared, and a sine function is assumed across pitch angle.

The spectral evolution of the flux is simulated separately for L = 5, 6, and 7. We assume each of these locations to be entirely outside of the plasmasphere, and therefore consider only chorus wave activity (Burtis & Helliwell, 1969; Meredith et al., 2014). In Equation 6, $D_{\alpha\alpha}$, D_{pp}, and $D_{p\alpha}$, are then the bounced averaged and half-drift averaged pitch angle, momentum, and mixed chorus diffusion coefficients. As we are only interested in the wave-particle interactions occurring on the dawn side, prior to the electrons

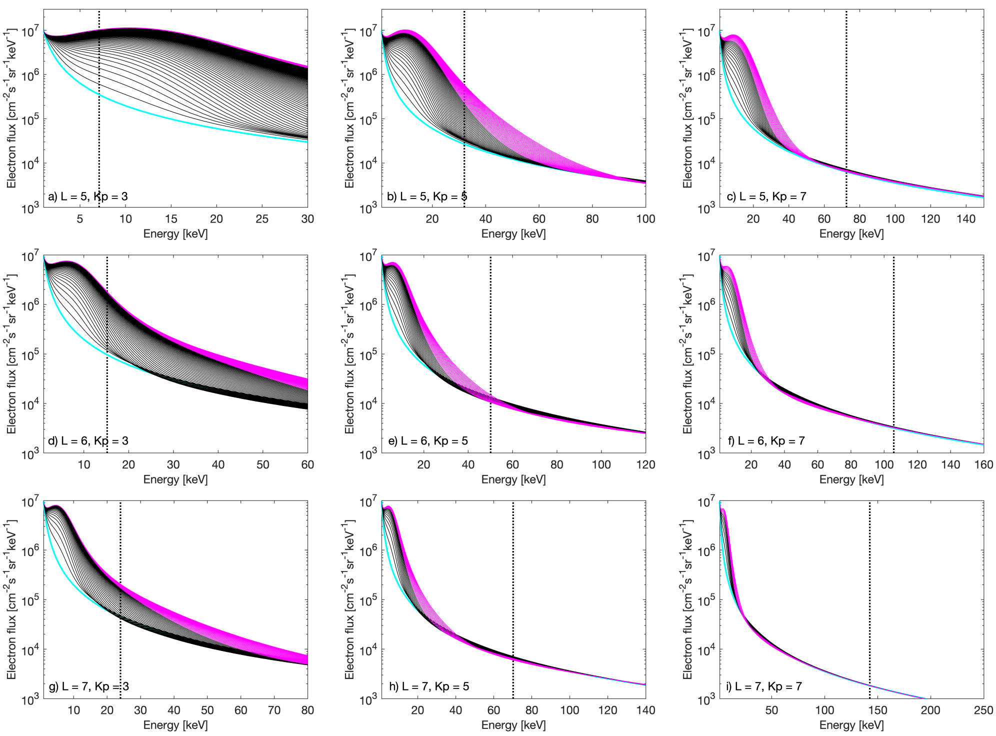

Figure 4. The evolution of electron flux across energy from chorus-driven diffusion in VERB-2D for electrons with an equatorial pitch angle of 75^o, starting from a soft initial energy distribution (cyan line). As the we are considering electron acceleration in the drift from the midnight sector through to noon, the chorus diffusion coefficients used are averaged over MLT = 0 -11. Panels a-c show the evolution at L = 5 for Kp = 3, 5, and 7 respectively. Panels d-e and g-i show the same Kp levels, but at L = 6 and L = 7 respectively. On each panel, the energy of an electron at the Alfvén layer at MLT of noon (for the specified L and Kp pair) is marked by a dotted vertical line. Flux distributions are shown in 3 minute intervals. Black lines correspond to the electron flux at times less than the time required for an electron at the Alfvén layer energy to drift from midnight to noon, and magenta lines mark times after this dawn drift period. Once a sufficient amount of time has lapsed for an electron at half the marked Alfvén layer energy to drift from midnight through to noon, we no longer plot the flux evolution from the VERB-2D simulation.

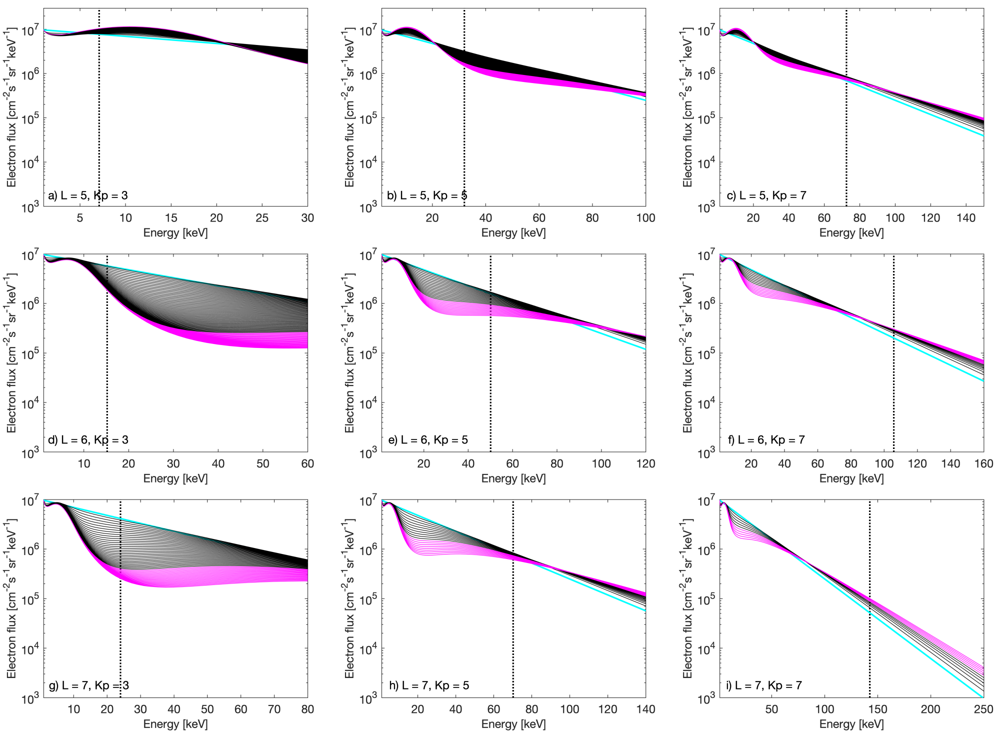

Figure 5. The evolution of the 75^o electron flux from VERB-2D starting with a hard intial condition (cyan line). The Figure takes the same format as Figure 4.

drifting out of the system, we calculate half-drift averaged diffusion coefficients over the dawn sector, between midnight and noon. Upper and lower band chorus diffusion coefficients are calculated in 1 hour MLT bins, between MLT = 00 and 11. All wave parameters in this calculation are taken from Wang et al. (2019), the magnetic field model is then given by a dipole model, and the electron plasma density is provided by the MLT and L dependent Sheeley et al. (2001) trough density model. We then average these MLT-binned diffusion coefficients using equal weighting to obtain the half-drift averaged coefficients (shown in Supplementary Figure S2).

Figure 4 shows the evolution of the VERB-2D electron flux at a pitch angle of 75^o from the soft initial spectrum. Three values of L (L= 5, 6, and 7) along with three values of Kp (Kp = 3, 5, and 7) are considered. For each Kp-L pair, a vertical dotted line marks the Alfvén layer energy at MLT=12 (calculated assuming K = 0 $G^{1/2}R_E$ in Section 2), providing an estimate of the energy threshold the electrons need to reach to be retained on a closed drift path. Electrons at energies to the left of this line would be on open drift paths. As discussed previously, the energisation is limited in time and must occur prior to the electrons drifting out of the system. We approximate this time frame as the time for electrons to drift from an MLT of midnight to noon (dawn-sector drift time), calculated in Section 3 and shown in Figure 3b-d. As can be seen from Figure 3b-d, the dawn-drift time is energy-dependent, with lower energies exhibiting longer drift time scales than higher energies. As electrons are energised by interactions with chorus waves, their drift speed will increase and the time available for chorus acceleration reduces. The minimum time available is the dawn-sector drift time of an electron starting at the Alfvén layer energy. In Figure 4, the initial condition is shown in cyan, and the flux distributions at subsequent times are shown in 3 minute intervals. Black lines mark the spectral evolution at times prior to the dawn-sector drift time for an electron at the Alfvén layer (i.e. before the minimum time available for acceleration). Magenta lines correspond to later times which are still less than the dawn-drift time scale for an electron starting at half of the Alfvén layer energy (e.g. for an Alfvén layer energy of 70 keV, the magenta lines would be times that are greater than the dawn-sector drift time of a 70 keV electron, but less than the dawn drift time of a 35 keV electron). Times longer than the dawn-drift for half the Alfvén layer energy are not shown.

From Figure 4a, d, and g we see that, for the lowest value of Kp considered, Kp = 3, the flux at the Alfvén layer energy increases on time scales less than the dawn-drift time of electrons at this threshold energy (black lines) for all three values of L, indicating that energization by chorus waves can act sufficiently quickly to contribute to the retention of the electrons on open drift paths. With increasing activity, the average chorus wave power is stronger, however, the Alfvén layer energy is also higher and as the electrons travel more rapidly through the dawn sector, the dawn-drift times shorter. At the highest activity modelled, Kp = 7, for all three values of L, we no longer observe an increase in the flux at, or past, the Alfvén layer energy during the necessary time frame. At Kp = 5, we see mixed behaviour between the different L values. At L = 5, the elec-

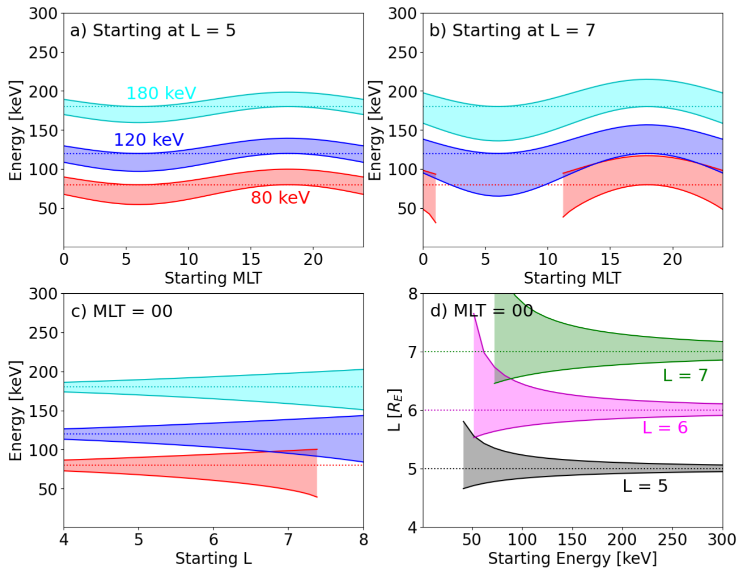

Figure 6. Assuming an electric field strength corresponding to Kp = 5 in the Maynard and Chen (1975) parametrisation of the Volland (1973);Stern (1975) electric field along with a dipole magnetic field, we show how parameters vary throughout the drift, for different starting conditions. Panel a shows how the minimum and maximum energies reached during the drift (upper and lower boundaries of the coloured regions) changes with the starting MLT, for 80 keV (red), 120 keV (blue), and 180 keV (cyan) electrons at $L = 5$. Panel b shows the same, but for $L = 7$. Note that at $L = 7$, electrons starting at 80 keV at MLTs between 01 and 11 do not complete closed drift paths, and so the minimum and maximum energies are not shown. Panel c shows how, for electrons initially at MLT = 00, the minimum and maximum energies reached varies with the initial L value. Finally, panel d shows the L coverage through the drift for different starting energies at MLT = 00. We consider initial L values of 5.0 (black), 6.0 (magenta), and 7 (green). Where an electron energy would not complete a closed drift, we do not plot the L coverage of the drift.

tron flux does increase at the Alfvén layer energy prior to the dawn-drift time. However, this is not observed for L= 6 or 7 where the Alfvén layer energies are larger.

The VERB-2D results shown in Figure 4, using the soft initial spectrum, indicate that chorus acceleration can contribute to the retention of electrons on open drift paths, but only during lower activity periods. Whether electron populations <300 keV exhibit an enhancement or loss due to interactions with chorus waves is sensitive to the initial gradients in phase space density (Allison et al., 2019; Horne et al., 2005). Figure 5 therefore shows the same simulations as Figure 4 but with a harder initial energy spectrum, given by the exponential function described above. In Figure 5, an increase in the flux at the Alfvén layer energy is now seen for Kp = 7 prior to the dawn-sector drift time of electrons starting at the Alfvén layer energy, for all three values of L (Figure 5c, f, and i). With the exception of Kp = 3, L = 5, where a small increase above the Alfvén layer energy is observed, at Kp = 3 and Kp = 5, flux at the energies surrounding the Alfvén layer now exhibit a net loss during the simulation due to pitch angle scattering. These results demonstrate that chorus wave-particle interactions can accelerate electrons originally on open drift paths such that they are retained and can be further energised over multiple drifts, but this is dependent on both the activity and the energy distributions of the low energy electrons.

A major assumption that we have made in the above analysis is that the electron energy is only changed by wave-particle interactions. As electrons drift around the Earth, their energy varies, conserving μ and K. Figure 6 shows this energy variation for an electric field configuration given by Kp = 5. Electrons originally on the dawn side decrease in energy as they traverse the dusk sector, while particles originally on the dusk side increase in energy as they move towards dawn; an effect magnified at larger radial distances. The energy change can become quite substantial ($\sim$ 50 keV) for electrons whose motion is notably impacted by the electric drifts (see Figure 6b, purple area). Chorus diffusion coefficients are, themselves, energy dependent, capturing how electrons of different energies resonate with the waves. Therefore the energy change throughout the drift may impact the spectral evolution resulting from chorus diffusion. Furthermore, Figure 6d shows how the L value varies through the drift for electrons of different energies. For $\sim$50 keV electrons starting at L = 6, MLT = 00, the minimum and maximum L value during the drift differ by ΔL $\approx$ 2. Chorus wave parameters and the plasma environment vary with spatial parameters such as MLT and L, impacting the overall effect of chorus wave-particle interactions (Wang et al., 2019; Horne et al., 2013). Electric field induced radial transport may therefore also influence the spectral evolution driven by diffusion. Additionally, as an electron is energised, the drift speed increases and the time available for chorus acceleration reduces. As discussed above, we have tried to mitigate this by considering the dawn-side drift time of the Aflvén energy, which serves as a minimum time frame for the acceleration. However, this caveat is addressed more thoroughly in the following section where we have incorporated the changing drift time into the simulation. We also have thus far only considered the Alfvén layer energies and drift times of equatorially mirroring electrons, calculated in Sections 2 and 3 assuming K = 0 $G^{1/2}R_E$. In the following section we also take into account the pitch angle dependence of the Alfvén layer energy and the drift speeds.

The energy change via the drift, the transport across L shells, and the decrease in the drift period resulting from energization cannot be included in a 2-D model. We therefore employ VERB-4D model to account for these factors.

5 Acceleration by chorus: VERB-4D

VERB-4D is a convection-diffusion code, solving the modified Fokker-Planck equation with convection terms (Shprits et al., 2015; Aseev et al., 2016, 2019). We have neglected radial diffusion, as we are interested in the evolution of the particle distribution as it drifts around the Earth solely due do interactions with chorus waves. We discuss this assumption further in the following section. VERB-4D solves

$$\begin{aligned}\frac{\partial f}{\partial t} &= -\langle v_\phi\rangle\frac{\partial f}{\partial \phi} - \langle v_{R_0}\rangle\frac{\partial f}{\partial R_0} + \frac{1}{G}\frac{\partial}{\partial V}G\left(D_{VV}\frac{\partial}{\partial V}f + D_{VK}\frac{\partial}{\partial K}f\right)\\ &\quad +\frac{1}{G}\frac{\partial}{\partial K}G\left(D_{KK}\frac{\partial}{\partial K}f + D_{VK}\frac{\partial}{\partial V}f\right) - \frac{f}{\tau}\end{aligned} \tag{8}$$

where, as in Equation 6, f is phase space density, t is time, and τ is the electron lifetime in the loss cone. The diffusion terms are now presented in terms of V and K, modified adiabatic invariants (Subbotin & Shprits, 2012), where $V = \mu(K{+}0.5)^2$ (μ is the first adiabatic invariant) and $K = J/\sqrt{8\mu m_0}$ (J is the second adiabatic invariant). D_{VV}, D_{VK}, and D_{KK} are the bounce averaged diffusion coefficients and G is the Jacobian of the coordinate transform from adiabatic invariants (μ, J,Φ) to (V,K,L), $G = -2\pi B_0(R_E^2/L^2)\sqrt{8m_0V}/(K+0.5)$ (Subbotin & Shprits, 2012). As in Section 2, B_0 denotes the magnetic field strength at the Earth's surface (taken to be $0.3{\times}10^{-4}$ T) and m_0 is the electron rest mass. The first two terms of Equation 8 are advection terms, accounting for the drift motion, where ϕ represents MLT and R_0 is the radial distance to a point on the geomagnetic equator. As we are operating in a dipole magnetic field, $R_0 = L$ for these simulations. We solve these advection terms using a ninth order upwinding scheme (Leonard, 1991), making use of a universal limiter and a discriminator (Leonard & Niknafs, 1991). The bounce-averaged drift velocities are given by $\langle v_\phi\rangle$ and $\langle v_{R_0}\rangle$ and are determined following a guiding centre approximation in a dipole magnetic field and Volland (1973);Stern (1975) electric field with the Maynard and Chen (1975) Kp parameterisation.

The radial boundaries of the simulation domain are set at $R_0 = 1R_E$ and $R_0 = 6.6R_E$, with $f = 0$ at the inner and outer boundary, simulating complete loss to the atmosphere and magnetopause along with no additional plasma sources. For the ϕ dimension, the boundary condition is periodic in MLT. Grid steps in R_0 and MLT are set to 0.1 R_E and 0.25 hours respectively. To construct the grid in V and K, a logarithmic grid in energy and a linear grid in pitch angle is set at the outer radial boundary (R_0 = 6.6 R_E) limited by 100 eV and 300 keV and 0.7^o and 89.3^o. The grid consists of 61 points in energy and 60 points in pitch angle. We then calculate V and K values on this grid, using a dipole magnetic field model, to determine the simulation grid. At maximum and minimum V boundaries, $\partial f/\partial V = 0$, allowing the phase space density values here to vary with the convection and diffusion. At the highest value of K (lowest equatorial pitch angle) we use $f = 0$ and at the lower boundary (highest equatorial pitch angle), $\partial f/\partial K = 0$.

A series of experiments are conducted using chorus diffusion coefficients from Wang et al. (2019), retaining the MLT dependence (the diffusion coefficients are calculated for every hour of MLT and interpolated onto the simulation MLT grid) and transforming from momentum and pitch angle to V and K space as described by Subbotin and Shprits (2012). These diffusion coefficients are scaled according to the chosen Kp level following the relations given by Wang et al. (2019). We have not included a plasmapause location and do not include scattering due to plasmaspheric hiss waves. An initial phase space density condition is constructed by setting the soft initial spectrum used in Section 4 at R_0 = 6.6 R_E for all MLT, and as before, assuming a sine dependence in pitch angle. This phase space density distribution is extended from R_0 = 6.6 R_E down to R_0 = 4 R_E by assuming a $R_0^{1/2}$ dependence in f (and $f = 0$ for $R_0 < 4$). To allow electrons outside the Alfvén layer to first be lost from the system, and MLT dependent energy and pitch angle distributions consistent with the electric field configuration to form, this initial phase space density was first evolved over two days in the absence of chorus diffusion. After this initial two-day "spin-up", chorus diffusion is activated and we explore the evolution of the phase space density over a further 24 hours, both in the absence of any further sources, and with a source of electrons at the MLT = 0 grid point, constructed to be only at V and K values entirely outside the Alfvén layer and so should

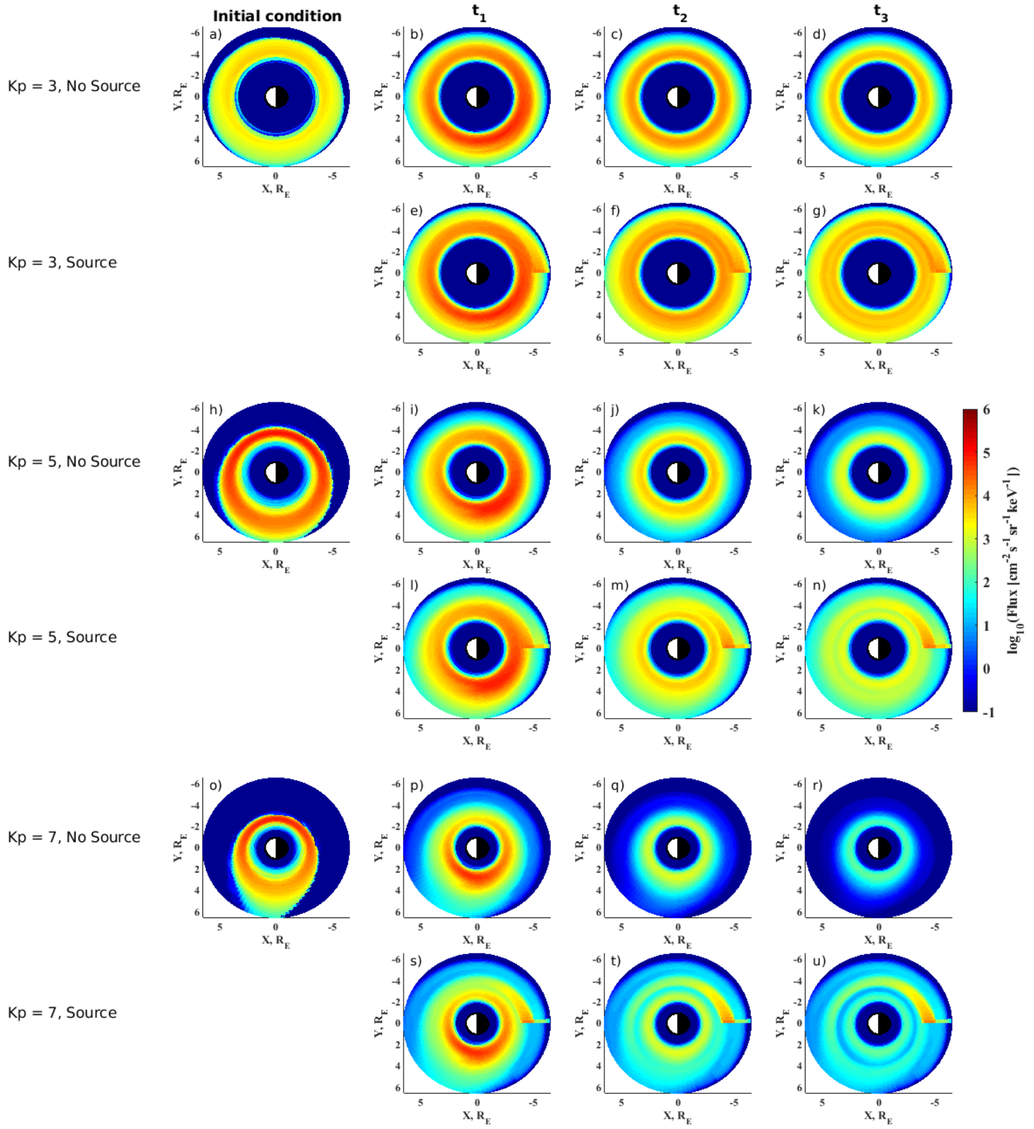

Figure 7. Electron flux at 30 keV, 75^o equatorial pitch angle from VERB-4D simulations. Panels a, h, and o show the electron flux following a 2 day 'spin-up' interval where the initial distribution was allowed to evolve under a Volland (1973);Stern (1975) electric field for Kp = 3, 5, and 7 respectively. These are labelled as 'initial condition' as they show the particle distribution prior to chorus waves being activated. Panels b-d, i-k, and p-r show snapshots of the how the 30 keV electron flux evolves, in the absence of a transient source population, at t_1 = 3 hours, t_2 = 11 hours, and t_3 = 19 hours, throughout the day of chorus wave activity, for Kp = 3, 5, and 7 respectively. At each of these activity levels, the flux from simulations including a transient source population, constructed to be entirely on open drift paths, is also shown in panels e-g, i-n, and s-u.

be lost on open drift paths. The source phase space density distribution is the same as the initial condition, set using the soft energy spectrum in Section 4 at R_0 = 6.6 R_E, with a sine distribution in pitch angle, and again extending this to $R_0 = 4$ (at energies where the Alfvén layer extends to $R_0 = 4$) by assuming a $R_0^{1/2}$ dependence in f.

Figure 7a shows the flux distribution at 30 keV and equatorial pitch angle 75^o immediately prior to chorus diffusion being activated in the VERB-4D simulation with a Volland (1973);Stern (1975) electric field set at Kp = 3. We use the scaling outlined in (Wang et al., 2019) and produce chorus diffusion coeffcients consistent with wave activity for Kp = 3. After 3 hours, 11 hours, and 19 hours (labelled t_1, t_2, and t_3 respectively), the flux distribution at 30 keV is shown, both for the simulation without the phase space density source (Figure 7b - d) and with the source (Figure 7e - g). Despite the source population being entirely outside the Alfvén layer, and therefore expected to be transient, lost within the drift period (see Supplementary Figure S3 which shows that, in the absence of chorus activity, this behaviour is observed) the 30 keV flux is higher in the simulation with the source than without, even after 19 hours have lapsed. The chorus waves have resulted in a portion of the sub-Alfvén layer source being retained in the simulation over multiple drifts.

We repeat the experiment using a Volland (1973);Stern (1975) electric field set at Kp = 5 and also at Kp = 7, and use chorus diffusion coefficients scaled accordingly. Figure 7h and o show the flux distributions at 30 keV and equatorial pitch angle 75^o for both simulations immediately prior to chorus diffusion being activated. For all three values of Kp shown, we have used the same initial phase space density distribution before allowing it to evolve under the electric field configuration in the two days without chorus diffusion, forming energy gradients in the phase space density consistent with the global field configuration. When chorus diffusion is activated, for both of Kp = 5 and 7, we again observe a higher flux in the simulation with a sub-Alfvén layer source, suggesting that, for these higher levels of activity, and therefore higher Alfvén layer energies and faster drift speeds, chorus still allows for a portion of the transient source population to be retained. Figure 7 shows that for Kp = 5 and 7, chorus wave activity mostly scatters the initial distribution at 30 keV, decreasing the flux with time; this effect is slowed by the inclusion of the sub-Alfvén Layer source. For Kp = 3, however, the flux initially increases due to the chorus waves (see Figure 7b and e at $t_1 = 3$ hours) and then decreases as the simulation progresses.

Figure 8 shows the time evolution of the 75^o flux distribution across energies at L = 5 and L = 6, where the flux has been averaged across all MLT points. Panels a-d show that for Kp = 3, an initial increase in flux arises over a broad range of energies due to the chorus wave interactions. Without the source on open drift paths, after ∼6 hours, the flux decreases at both L = 5 and L = 6 for energies <100 keV. With the source on open drift paths, the decrease at <100 keV is greatly reduced. At Kp = 3, both with and without the source on open drift paths, the >200 keV flux has increased from the initial condition at L = 5 and L = 6, showing that chorus waves have resulted in a net acceleration at these energies. This flux increase is larger when the source population on open drifts is present.

At Kp = 5, Figure 8e-h shows that for energies <100 keV the flux mostly decreases during the simulation at both L = 5 and L = 6. When including a source of electrons on open drift paths, the <100 keV flux shows a smaller decrease than when the source was not present and, for energies >200 keV, the flux at the end of the 1-day simulation is larger than the initial condition, showing a net increase. In the absence of the supplied source population, a net decrease is instead seen for energies >200 keV, demonstrating that the part of the supplied source is accelerated before being lost on open drift paths. At Kp = 7, similar behaviour is observed (Figure 8i-l). Again, when the source population is present, slower loss due to chorus wave scattering occurs which ultimately stabilises and, when averaged over all MLT, shows little change after the first 3 hours. Without the source population on open drift paths, the electron flux decreases throughout the run. At L=6, we again observe an increase from the initial condition for energies >150

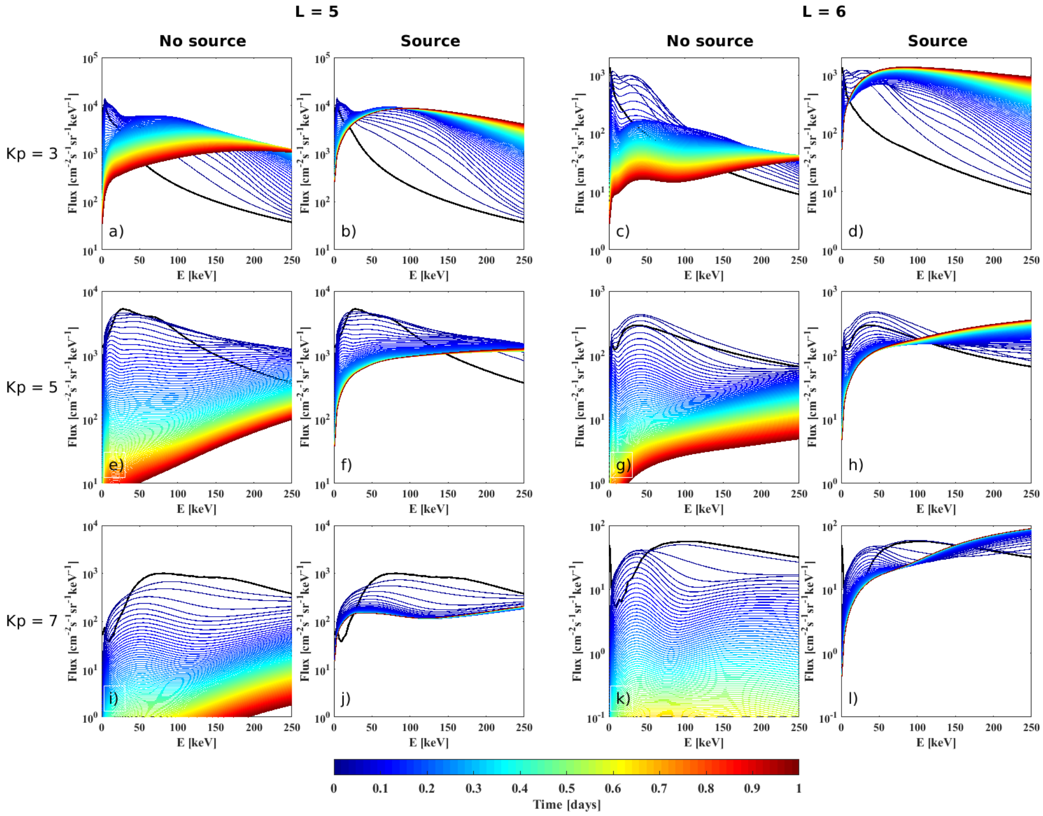

Figure 8. Time evolution of the electron flux distribution across energy at 75^o pitch angle, averaged over all magnetic local time points, for the chorus-driven diffusion in VERB-4D. The line colors indicate different times in the one day period and the initial condition for the electron flux is shown as a thick black line. We show the MLT-averaged energy distribution evolution, both with and without the the transient source, at L = 5 and L =6, for Kp = 3 (a-d), Kp = 5 (e-h), and Kp = 7 (i-l).

keV when the source population on open drift paths is present (panel l), but a net decrease without (panel k).

6 Discussion

The results in Section 4 and 5 show that in both the 2-D and 4-D simulations, the chorus acceleration time can be faster than the time for electrons below the Alfvén layer to drift out of the region. As a result, a portion of electrons which, in the absence of chorus interactions, would be on open drift paths and lost from the system, can be retained and present a seed population for further acceleration to radiation belt energies (Jaynes et al., 2015). The acceleration time for electrons <300 keV can depend on the energy distribution of the electron population, and we find that whether chorus interactions accelerate electrons to above the Alfvén layer energy within their drift time is dependent on the spectral shape. Further work is required to determine the typical energy spectrum of electrons supplied to the radiation belt region.

In Section 2, we showed that electrons which were originally on the dusk side for the convection electric field enhancement can remain trapped down to much lower energies than those starting on the dawn side. Additionally, Figure 6 shows that for high Kp, this pre-existing dusk side seed population could gain an additional 40 - 50 keV as it drifts to the dawn side where chorus waves are most active (Meredith et al., 2014). Furthermore, owing to the drift speeds, a given particle on a closed drift will spend longer on the dusk side of the Earth than the dawn, as seen in Figure 3, where the total drift time marginally increased with Kp while the dawn sector drift time reduced with increasing Kp. As such, it may be that the >60 keV electron populations (Figure 2 shows an Alfvén layer energy of ∼60 keV for Kp = 7 in the dusk sector for much of the outer radiation belt region) already present in the ring current prior to the activity enhancement can notably contribute to the seed population that is accelerated to higher energies. A similar discussion was presented by Califf et al. (2017) in the context of slot region filling.

As discussed in the introduction, we make the assumption that the fields remain static throughout the drift time. In reality this is unlikely to be the case and both the electric and magnetic field will vary, altering the electron drift paths. However, by assuming static fields in this work, we explore the contribution of chorus waves alone in altering the electron drift trajectories. Time-variations in the electric and magnetic fields on timescales shorter than particle drift periods can retain portions of the populations originally on open drift paths. Further research is required to determine the relative contribution of chorus acceleration in comparison to large scale field fluctuations in the retention of electrons as well as the effect of these processes occurring together. Steady magnetospheric convection (SMC) events present extended periods of enhanced convection, and storms with SMC events in the recovery phase are more likely to increase relativistic electron flux levels (Kissinger et al., 2014). The elevated chorus activity during these events may contribute to accelerating a portion of electrons on open drift paths up to energies that encircle the Earth. These populations can then contribute to a seed population for relativistic electron flux enhancements.

In this study, we have only considered the acceleration due to electron interactions with chorus waves. Ultra-low frequency (ULF) waves can also interact drift-resonantly with electrons, resulting in transport and energisation (Ozeke et al., 2012). Further work is required to determine how these ULF waves interact with electrons which do not complete a full drift around the Earth and if this interaction can also energise electrons sufficiently quickly so as to help retain populations on open drift paths. Additionally, Lejosne et al. (2018) showed that sub-auroral polarisation streams (SAPS) can inject electrons with energies of tens to hundreds of keV down to lower radial distances, increasing the energy. The presence of SAPS may therefore also help contribute to the retention of electrons below the Alfvén layer, a factor we have not considered in this work. Chorus acceleration may therefore more readily contribute to the retention of populations on open drift paths than indicated in this work when SAPS are taken into account. The acceleration time scales for chorus induced diffusion can vary due to changing wave and plasma parameters. The diffusion coefficients we use for this analysis utilise the Sheeley et al. (2001) density model. Recent work has shown density variations not captured by the Sheeley et al. (2001) model during active periods that result in increased chorus acceleration, right up to ultra-relativistic energies (Allison et al., 2021). As a result, during active periods that show strong depletions in the electron density, interactions with chorus waves may more rapidly energize electrons, retaining a larger portion of the populations on open drift paths.

7 Conclusions

In this study, we explore whether interactions with chorus waves can accelerate electrons on open drift trajectories to energies above the Alfvén layer prior to them leaving the system. Drift trajectories, electron energies on closed drift paths, and drift time scales were calculated by making use of (U,B,K) space (Whipple Jr., 1978), using a Volland

(1973);Stern (1975) electric field (with the Maynard and Chen (1975) Kp parameterisation) and a dipole magnetic field. Acceleration timescales from resonant interactions with whistler mode chorus waves were calculated with the VERB-2D model, employing quasi-linear diffusion theory to treat the wave particle interactions as a diffusion of electron phase space density across energy and pitch angles. We compare the drift and acceleration timescales from both a hard and soft initial energy spectrum for Kp = 3, 5, and 7 at L = 5, 6, and 7. We then further this analysis by utilizing the full convection-diffusion model of VERB-4D, again with a Volland (1973);Stern (1975) electric field and dipole magnetic field. Using MLT dependent chorus diffusion coefficients, we explore the evolution of the electron populations both with and without the inclusion of a source population at MLT = 0, constructed to be entirely on open drift trajectories. Our main conclusions are as follows:

1. The energies of electrons which are on open drift paths can vary substantially between the dawn and dusk magnetic local time sectors at the same radial distance. For Kp > 7, the Alfvén layer energy can be in excess of 125 keV in the dawn side outer radiation belt region of L = 4-6, while at the corresponding L in the dusk MLT sector, Alfvén layer energies are $\sim$60 keV.
2. With increasing convection electric field, the drift speed in the dawn sector increases and electrons travel from night side to the day side more rapidly. However, as the convection electric field increases, the total drift time for an electron increases as electrons spend more time on the dusk side of the Earth.
3. Via 2-D simulations in momentum and pitch angle, we demonstrate that chorus wave particle interactions can accelerate electrons to the Alfvén layer energy and above on timescales less than the time taken for an electron at the Alfvén layer energy to drift from midnight, through dawn, to noon. However, this acceleration timescale depends on the initial energy distribution of the electron populations, and whether chorus acceleration can contribute to retaining electrons on open drift paths depends on the energy spectrum.
4. In 4-D simulations, we find a higher electron flux over a range of energies when a source population was included that was entirely below the Alfvén layer energies, suggesting that a portion of this source population is being accelerated before it is lost from the region.

The results presented in this paper demonstrate that, even in the absence of large scale field changes, energetic electron populations on open drift paths may not be fully transient due to energisation by chorus waves.

Acknowledgments

No satellite data is used in this study. All conclusions are drawn based on calculations performed in U,B,K space or numerical model simulations. This work was funded by the Alexander von Humboldt foundation. Y.Y.S. and M.W. acknowledge support from the European Union's Horizon 2020 research and innovation programme under grant agreement No. 870452 (PAGER).. R.B.H. and S.A.G. were supported by NERC Highlight Topic Grant NE/P01738X/1 (Rad-Sat).

References

Allison, H. J., Horne, R. B., Glauert, S. A., & Del Zanna, G. (2019). On the importance of gradients in the low-energy electron phase space density for relativistic electron acceleration. *Journal of Geophysical Research: Space Physics*, *124*(4), 2628-2642. Retrieved from `https://agupubs.onlinelibrary.wiley.com/doi/abs/10.1029/2019JA026516` doi: https://doi.org/10.1029/2019JA026516

Allison, H. J., Horne, R. B., Glauert, S. A., & Zanna, G. D. (2017). The magnetic local time distribution of energetic electrons in the radiation belt region. *Journal of Geophysical Research: Space Physics*, *122*(8), 8108-8123. Retrieved from https://agupubs.onlinelibrary.wiley.com/doi/abs/10.1002/2017JA024084 doi: https://doi.org/10.1002/2017JA024084

Allison, H. J., Shprits, Y. Y., Zhelavskaya, I. S., Wang, D., & Smirnov, A. G. (2021). Gyroresonant wave-particle interactions with chorus waves during extreme depletions of plasma density in the van allen radiation belts. *Science Advances*, *7*(5), eabc0380. Retrieved from https://www.science.org/doi/abs/10.1126/sciadv.abc0380 doi: 10.1126/sciadv.abc0380

Aseev, N. A., Shprits, Y. Y., Drozdov, A. Y., & Kellerman, A. C. (2016). Numerical applications of the advective-diffusive codes for the inner magnetosphere. *Space Weather*, *14*(11), 993-1010. Retrieved from https://agupubs.onlinelibrary.wiley.com/doi/abs/10.1002/2016SW001484 doi: https://doi.org/10.1002/2016SW001484

Aseev, N. A., Shprits, Y. Y., Wang, D., Wygant, J., Drozdov, A. Y., Kellerman, A. C., & Reeves, G. D. (2019). Transport and loss of ring current electrons inside geosynchronous orbit during the 17 march 2013 storm. *Journal of Geophysical Research: Space Physics*, *124*(2), 915-933. Retrieved from https://agupubs.onlinelibrary.wiley.com/doi/abs/10.1029/2018JA026031 doi: https://doi.org/10.1029/2018JA026031

Bingham, S. T., Mouikis, C. G., Kistler, L. M., Paulson, K. W., Farrugia, C. J., Huang, C. L., … Kletzing, C. (2019). The storm time development of source electrons and chorus wave activity during cme- and cir-driven storms. *Journal of Geophysical Research: Space Physics*, *124*(8), 6438-6452. Retrieved from https://agupubs.onlinelibrary.wiley.com/doi/abs/10.1029/2019JA026689 doi: 10.1029/2019JA026689

Borovsky, J. E., & Cayton, T. E. (2011). Entropy mapping of the outer electron radiation belt between the magnetotail and geosynchronous orbit. *Journal of Geophysical Research: Space Physics*, *116*(A6). Retrieved from https://agupubs.onlinelibrary.wiley.com/doi/abs/10.1029/2011JA016470 doi: https://doi.org/10.1029/2011JA016470

Burin des Roziers, E., Li, X., Baker, D. N., Fritz, T. A., Friedel, R., Onsager, T. G., & Dandouras, I. (2009). Energetic plasma sheet electrons and their relationship with the solar wind: A cluster and geotail study. *Journal of Geophysical Research: Space Physics*, *114*(A2). Retrieved from https://agupubs.onlinelibrary.wiley.com/doi/abs/10.1029/2008JA013696 doi: https://doi.org/10.1029/2008JA013696

Burtis, W. J., & Helliwell, R. A. (1969). Banded chorus—a new type of vlf radiation observed in the magnetosphere by ogo 1 and ogo 3. *Journal of Geophysical Research (1896-1977)*, *74*(11), 3002-3010. Retrieved from https://agupubs.onlinelibrary.wiley.com/doi/abs/10.1029/JA074i011p03002 doi: https://doi.org/10.1029/JA074i011p03002

Califf, S., Li, X., Zhao, H., Kellerman, A., Sarris, T. E., Jaynes, A., & Malaspina, D. M. (2017). The role of the convection electric field in filling the slot region between the inner and outer radiation belts. *Journal of Geophysical Research: Space Physics*, *122*(2), 2051-2068. Retrieved from https://agupubs.onlinelibrary.wiley.com/doi/abs/10.1002/2016JA023657 doi: 10.1002/2016JA023657

DeForest, S. E., & McIlwain, C. E. (1971). Plasma clouds in the magnetosphere. *Journal of Geophysical Research (1896-1977)*, *76*(16), 3587-3611. Retrieved from https://agupubs.onlinelibrary.wiley.com/doi/abs/10.1029/JA076i016p03587 doi: https://doi.org/10.1029/JA076i016p03587

Glauert, S. A., Horne, R. B., & Meredith, N. P. (2014). Three-dimensional electron radiation belt simulations using the bas radiation belt model with new diffusion models for chorus, plasmaspheric hiss, and lightning-generated whistlers. *Journal of Geophysical Research: Space Physics*, *119*, 268-289. doi: 10.1002/2013JA019281

Horne, R. B., Kersten, T., Glauert, S. A., Meredith, N. P., Boscher, D., Sicard-Piet, A., ... Li, W. (2013). A new diffusion matrix for whistler mode chorus waves. *Journal of Geophysical Research: Space Physics*, *118*(10), 6302-6318. Retrieved from `https://agupubs.onlinelibrary.wiley.com/doi/abs/10.1002/jgra.50594` doi: https://doi.org/10.1002/jgra.50594

Horne, R. B., Thorne, R. M., Glauert, S. A., Albert, J. M., Meredith, N. P., & Anderson, R. R. (2005). Timescale for radiation belt electron acceleration by whistler mode chorus waves. *Journal of Geophysical Research: Space Physics*, *110*(A3). Retrieved from `https://agupubs.onlinelibrary.wiley.com/doi/abs/10.1029/2004JA010811` doi: 10.1029/2004JA010811

Jaynes, A. N., Baker, D. N., Singer, H. J., Rodriguez, J. V., Loto'aniu, T. M., Ali, A. F., ... Reeves, G. D. (2015). Source and seed populations for relativistic electrons: Their roles in radiation belt changes. *Journal of Geophysical Research: Space Physics*, *120*(9), 7240-7254. Retrieved from `https://agupubs.onlinelibrary.wiley.com/doi/abs/10.1002/2015JA021234` doi: https://doi.org/10.1002/2015JA021234

Kennel, C. F., & Engelmann, F. (1966). Velocity space diffusion from weak plasma turbulence in a magnetic field. *The Physics of Fluids*, *9*(12), 2377-2388. Retrieved from `https://aip.scitation.org/doi/abs/10.1063/1.1761629` doi: 10.1063/1.1761629

Kissinger, J., Kepko, L., Baker, D. N., Kanekal, S., Li, W., McPherron, R. L., & Angelopoulos, V. (2014). The importance of storm time steady magnetospheric convection in determining the final relativistic electron flux level. *Journal of Geophysical Research: Space Physics*, *119*(9), 7433-7443. Retrieved from `https://agupubs.onlinelibrary.wiley.com/doi/abs/10.1002/2014JA019948` doi: https://doi.org/10.1002/2014JA019948

Korth, H., & Thomsen, M. F. (2001). Plasma sheet access to geosynchronous orbit: Generalization to numerical global field models. *Journal of Geophysical Research: Space Physics*, *106*(A12), 29655-29667. Retrieved from `https://agupubs.onlinelibrary.wiley.com/doi/abs/10.1029/2000JA000373` doi: 10.1029/2000JA000373

Korth, H., Thomsen, M. F., Borovsky, J. E., & McComas, D. J. (1999). Plasma sheet access to geosynchronous orbit. *Journal of Geophysical Research: Space Physics*, *104*(A11), 25047-25061. Retrieved from `https://agupubs.onlinelibrary.wiley.com/doi/abs/10.1029/1999JA900292` doi: 10.1029/1999JA900292

Lejosne, S., Kunduri, B. S. R., Mozer, F. S., & Turner, D. L. (2018). Energetic electron injections deep into the inner magnetosphere: A result of the subauroral polarization stream (saps) potential drop. *Geophysical Research Letters*, *45*(9), 3811-3819. Retrieved from `https://agupubs.onlinelibrary.wiley.com/doi/abs/10.1029/2018GL077969` doi: https://doi.org/10.1029/2018GL077969

Leonard, B., & Niknafs, H. (1991). Sharp monotonic resolution of discontinuities without clipping of narrow extrema. *Computers and Fluids*, *19*(1), 141-154. Retrieved from `https://www.sciencedirect.com/science/article/pii/0045793091900116` (Special Issue CTAC-89) doi: https://doi.org/10.1016/0045-7930(91)90011-6

Leonard, B. P. (1991, June). The ULTIMATE conservative difference scheme applied to unsteady one-dimensional advection. *Computer Methods in Applied Mechanics and Engineering*, *88*(1), 17-74. doi: 10.1016/0045-7825(91)90232-U

Lyons, L., & Williams, D. (1984). *Quantitative aspects of magnetospheric physics.* Springer, Dordrecht. Retrieved from `https://doi.org/10.1007/978-94-017`

-2819-5
Maynard, N. C., & Chen, A. J. (1975). Isolated cold plasma regions: Observations and their relation to possible production mechanisms. *Journal of Geophysical Research (1896-1977)*, *80*(7), 1009-1013. Retrieved from https://agupubs.onlinelibrary.wiley.com/doi/abs/10.1029/JA080i007p01009 doi: 10.1029/JA080i007p01009

Meredith, N. P., Horne, R. B., Li, W., Thorne, R. M., & Sicard-Piet, A. (2014). Global model of low-frequency chorus (flhr¡f¡0.1fce) from multiple satellite observations. *Geophysical Research Letters*, *41*(2), 280-286. Retrieved from https://agupubs.onlinelibrary.wiley.com/doi/abs/10.1002/2013GL059050 doi: https://doi.org/10.1002/2013GL059050

Mouikis, C. G., Bingham, S. T., Kistler, L. M., Farrugia, C. J., Spence, H. E., Reeves, G. D., ... Kletzing, C. A. (2019). The storm-time ring current response to icmes and cirs using van allen probe observations. *Journal of Geophysical Research: Space Physics*, *124*(11), 9017-9039. Retrieved from https://agupubs.onlinelibrary.wiley.com/doi/abs/10.1029/2019JA026695 doi: 10.1029/2019JA026695

Orlova, K., & Shprits, Y. (2014, 2). Model of lifetimes of the outer radiation belt electrons in a realistic magnetic field using realistic chorus wave parameters. *Journal of Geophysical Research A: Space Physics*, *119*, 770-780. doi: 10.1002/2013JA019596

Ozeke, L. G., Mann, I. R., Murphy, K. R., Rae, I. J., Milling, D. K., Elkington, S. R., ... Singer, H. J. (2012). Ulf wave derived radiation belt radial diffusion coefficients. *Journal of Geophysical Research: Space Physics*, *117*(A4). Retrieved from https://agupubs.onlinelibrary.wiley.com/doi/abs/10.1029/2011JA017463 doi: https://doi.org/10.1029/2011JA017463

Roederer, J. G. (1967). On the adiabatic motion of energetic particles in a model magnetosphere. *Journal of Geophysical Research (1896-1977)*, *72*(3), 981-992. Retrieved from https://agupubs.onlinelibrary.wiley.com/doi/abs/10.1029/JZ072i003p00981 doi: https://doi.org/10.1029/JZ072i003p00981

Sheeley, B. W., Moldwin, M. B., Rassoul, H. K., & Anderson, R. R. (2001). An empirical plasmasphere and trough density model: Crres observations. *Journal of Geophysical Research: Space Physics*, *106*(A11), 25631-25641. Retrieved from https://agupubs.onlinelibrary.wiley.com/doi/abs/10.1029/2000JA000286 doi: https://doi.org/10.1029/2000JA000286

Shprits, Y. Y., Elkington, S. R., Meredith, N. P., & Subbotin, D. A. (2008). Review of modeling of losses and sources of relativistic electrons in the outer radiation belt i: Radial transport. *Journal of Atmospheric and Solar-Terrestrial Physics*, *70*(14), 1679-1693. Retrieved from https://www.sciencedirect.com/science/article/pii/S1364682608001648 (Dynamic Variability of Earth's Radiation Belts) doi: https://doi.org/10.1016/j.jastp.2008.06.008

Shprits, Y. Y., Kellerman, A. C., Drozdov, A. Y., Spence, H. E., Reeves, G. D., & Baker, D. N. (2015). Combined convective and diffusive simulations: Verb-4d comparison with 17 march 2013 van allen probes observations. *Geophysical Research Letters*, *42*(22), 9600-9608. Retrieved from https://agupubs.onlinelibrary.wiley.com/doi/abs/10.1002/2015GL065230 doi: https://doi.org/10.1002/2015GL065230

Shprits, Y. Y., Subbotin, D. A., Meredith, N. P., & Elkington, S. R. (2008). Review of modeling of losses and sources of relativistic electrons in the outer radiation belt ii: Local acceleration and loss. *Journal of Atmospheric and Solar-Terrestrial Physics*, *70*(14), 1694-1713. Retrieved from https://www.sciencedirect.com/science/article/pii/S1364682608001673 (Dynamic Variability of Earth's Radiation Belts) doi: https://doi.org/10.1016/j.jastp.2008.06.014

Stern, D. P. (1975). The motion of a proton in the equatorial magnetosphere.

Journal of Geophysical Research (1896-1977), *80*(4), 595-599. Retrieved from https://agupubs.onlinelibrary.wiley.com/doi/abs/10.1029/JA080i004p00595 doi: 10.1029/JA080i004p00595

Su, Z., Xiao, F., Zheng, H., & Wang, S. (2010). Steerb: A three-dimensional code for storm-time evolution of electron radiation belt. *Journal of Geophysical Research: Space Physics*, *115*. doi: 10.1029/2009JA015210

Subbotin, D. A., & Shprits, Y. Y. (2012). Three-dimensional radiation belt simulations in terms of adiabatic invariants using a single numerical grid. *Journal of Geophysical Research: Space Physics*, *117*(A5). Retrieved from https://agupubs.onlinelibrary.wiley.com/doi/abs/10.1029/2011JA017467 doi: https://doi.org/10.1029/2011JA017467

Subbotin, D. A., Shprits, Y. Y., Gkioulidou, M., Lyons, L. R., Ni, B., Merkin, V. G., ... Hudson, M. K. (2011). Simulation of the acceleration of relativistic electrons in the inner magnetosphere using rcm-verb coupled codes. *Journal of Geophysical Research: Space Physics*, *116*. doi: 10.1029/2010JA016350

Thorne, R. M., Shprits, Y. Y., Meredith, N. P., Horne, R. B., Li, W., & Lyons, L. R. (2007). Refilling of the slot region between the inner and outer electron radiation belts during geomagnetic storms. *Journal of Geophysical Research: Space Physics*, *112*(A6). Retrieved from https://agupubs.onlinelibrary.wiley.com/doi/abs/10.1029/2006JA012176 doi: https://doi.org/10.1029/2006JA012176

Volland, H. (1973). A semiempirical model of large-scale magnetospheric electric fields. *Journal of Geophysical Research (1896-1977)*, *78*(1), 171-180. Retrieved from https://agupubs.onlinelibrary.wiley.com/doi/abs/10.1029/JA078i001p00171 doi: 10.1029/JA078i001p00171

Walt, M. (1994). *Introduction to geomagnetically trapped radiation* (Vol. 10). Cambridge University Press.

Wang, D., & Shprits, Y. Y. (2019). On how high-latitude chorus waves tip the balance between acceleration and loss of relativistic electrons. *Geophysical Research Letters*, *46*(14), 7945-7954. Retrieved from https://agupubs.onlinelibrary.wiley.com/doi/abs/10.1029/2019GL082681 doi: https://doi.org/10.1029/2019GL082681

Wang, D., Shprits, Y. Y., Zhelavskaya, I. S., Agapitov, O. V., Drozdov, A. Y., & Aseev, N. A. (2019). Analytical chorus wave model derived from van allen probe observations. *Journal of Geophysical Research: Space Physics*, *124*(2), 1063-1084. Retrieved from https://agupubs.onlinelibrary.wiley.com/doi/abs/10.1029/2018JA026183 doi: https://doi.org/10.1029/2018JA026183

Whipple Jr., E. C. (1978). (u, b, k) coordinates: A natural system for studying magnetospheric convection. *Journal of Geophysical Research: Space Physics*, *83*(A9), 4318-4326. Retrieved from https://agupubs.onlinelibrary.wiley.com/doi/abs/10.1029/JA083iA09p04318 doi: 10.1029/JA083iA09p04318